Chapter 4

First Principle Evaluation of Photocatalytic Suitability for TiO_2-Based Nanotubes

Yuri F. Zhukovskii, Sergey Piskunov, Oleg Lisovski, Andrei Chesnokov and Dmitry Bocharov

Additional information is available at the end of the chapter

http://dx.doi.org/10.5772/63236

Abstract

Water splitting under the influence of solar light on semiconducting electrodes Immersed in aqueous electrolyte is a potentially clean and renewable source for hydrogen fuel production. Its efficiency depends on relative position of the band gap edges (the visible light interval between infrared and ultraviolet (UV) ranges of electromagnetic spectrum corresponds to gap widths 1.5–2.8 eV) accompanied by a proper band alignment relative to both reduction (H^+/H_2) and oxidation (O_2/H_2O) potentials (−4.44 eV and −5.67 eV on energy scale for vacuum, respectively) which must be positioned inside the band gap. Its width for TiO_2 anatase-structured bulk is experimentally found to be 3.2 eV, which corresponds to photocatalytic activity under UV light possessing only ~1% efficiency of sunlight energy conversion. Noticeable growth of this efficiency can be achieved by by adjusting the band gap edges for titania bulk through nanoscale transformation of its morphology to anatase-type nanotubes (NTs) (formed by folding of (001) or (101) nanothin TiO_2 sheets consisting of 9 or 6 atomic layers and possessing either (n,0) or (−n,n) chiralities, respectively) accompanied by partial substitution of pristine atoms by C_O, Fe_{Ti}, N_O and S_O single dopants as well as N_O+S_O codopants. In the latter case, the band gap can be reduced down to 2.2 eV while the efficiency is achieved up to ~15%. The energy differences between the edges of band gap (VB and CB), the highest occupied and lowest unoccupied impurity levels inside the band gap (HOIL and LUIL, respectively) induced in doped NTs, while preserving the proper disposition of these levels relatively to the redox potentials, so that $\varepsilon_{VB} < \varepsilon_{HOIL} < \varepsilon_{O_2/H_2O} < \varepsilon_{H^+/H_2} < \varepsilon_{LUIL} < \varepsilon_{CB}$, thus reducing the photon energy required for dissociation of H_2O molecule. In this chapter, we analyze applicability of large-scale first principle calculations on the doped single-wall titania NTs of different morphologies with the aim of establishment of their suitability for photocatalytic water splitting.

Keywords: titania anatase-structured nanotubes, (001) vs. (101) polylayer single-wall morphologies, (*n*,0) vs. (−*n*,*n*) chirality, C_O, Fe_{Ti}, N_O and S_O substitutional dopants, electronic structure, photocatalytic suitability, *ab initio* hybrid DFT+HF calculations

1. Introduction

Finding alternative energy sources is one of the most urgent research problems since traditional fuels run out at an extreme rate as their depleting rate surpasses the rate of restoration. Photocatalytic dissociation of H_2O molecules under the influence of solar light on a semiconductor electrode is a very promising process for production of hydrogen fuel, which is an environmentally friendly energy source. Indeed, the only combustion product of H_2 is water, while traditional hydrogen production technologies (e.g., steam reforming) are accompanied by CO_2 release and/or other undesirable side products. Another advantage of hydrogen as energy carrier is its high energy density ~237 kJ/mol [1]. On the other hand, among different energy sources surrounding people, the Sun is the most abundant – approximately 3.0×10^{24} J of its emitted energy reaches the Earth every year. In turn, the humanity consumes around 4.0×10^{20} J [2], so advances in technology are required to converse, use and store the solar energy with high efficiency. Moreover, photocatalysis is often considered as artificial photosynthesis and as such is an attractive and challenging research topic in the fields of contemporary chemistry and renewable energetics [3, 4].

In this chapter, we systematize, analyze and verify, systematize and analyze the results obtained using first principle calculations on the atomic and electronic structure of pristine and doped by C_O, Fe_{Ti}, N_O and S_O substitutes TiO_2 anatase-structured single-wall nanotubes (SW NTs). Their chirality vectors are perpendicular to (001) and (101) nanosheets consisting of 9 or 6 layers, respectively, while chirality indexes have been chosen among (*n*,0) vs. (−*n*,*n*) sets, respectively. Evaluation of photocatalytic suitability of all titania NTs simulated by us has been performed taking into account their correspondence to band gaps, widths of which are smaller than photon energies in visible light interval while redox levels H^+/H_2 and O_2/H_2O (−4.44 and −5.67 eV, respectively) are positioned inside these band gaps. This chapter is based on results of our own studies [5–9] as well as theoretical and experimental data available in the literature.

2. Literature review

2.1. Fundamentals of water photocatalytic splitting

In the first publication on water photocatalytic splitting, Honda and Fujishima managed to split water into oxygen and hydrogen using rutile-structured TiO_2 anode and platinum cathode [10], both immersed into water electrolyte solution. Since titania bulk samples were

http://dx.doi.org/10.5772/63236

found to be suited for solar energy conversion, they attracted a great attention in electrochemical technologies. **Figure 1** clearly illustrates the mechanism of photocatalytic splitting.

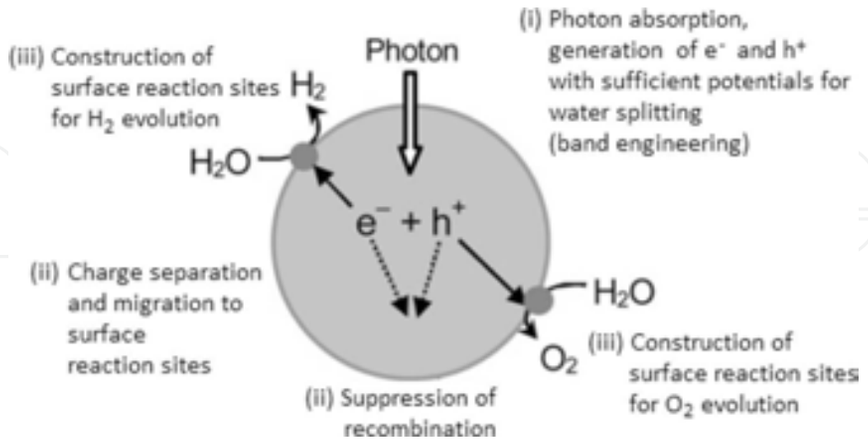

Figure 1. Elemental stages of photocatalytic water splitting [4].

In the first stage, a photon is absorbed by a semiconductor electrode (anode) which leads to generation of excitons – pairs of excited electrons and electron holes (second stage). Electrons being excited migrate to a conduction band (CB), and electron holes stay in a valence band (VB). The third stage includes charge separation and migration to reaction centers on a catalyst's or cocatalyst's surface. Usually cocatalyst is used because in that case photoanode and cathode, i.e., areas where hydrogen and oxygen are generated, are divided, and the backward reaction between the gases cannot happen. Another important aspect is that the kinetics of electron transfer on a semiconductor surface may cause a necessity of the cocatalyst presence (such as Pt, NiO or RuO_2), which can suppress charge recombination (fourth stage) occurring mainly due to the presence of irregularities in the semiconductor crystalline structure. The fifth stage results in the appearance of reaction centers on the electrode substrate. A better understanding of the whole water-splitting process can be gained from **Figure 2**.

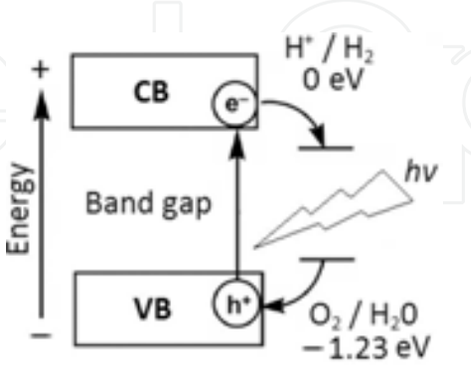

Figure 2. The model of photocatalytic activity of semiconducting electrode [4].

Fundamental requirement to an electrode is to be a semiconductor possessing band gap in the energy spectrum which cannot be passed by the compound's electrons. Normally, they are

localized at the ground states below the top of the band gap. But, when an electron receives additional portion of energy from an external source (for example, due to rising temperature or light photon absorption), which is sufficient to overcome the band gap – the electron turns into an excited state, above the bottom of CB (**Figure 2**), while an electron hole (positive charge carrier) is left in a VB. An electron cannot exist in an excited (metastable) state for a long time – it is not energetically beneficial. This is why electrons transferred to a CB tend to get rid of energy surplus (e.g., by irradiating it) and to return back into their ground state in a VB.

The next requirement is connected with the positions of the CB and the VB on energy scale. The bottom of the CB must be situated slightly higher than the standard hydrogen electrode (SHE) level (0 V, or −4.44 eV, in compliance with vacuum level) as shown in **Figure 2**, so the following reaction is energetically favorable in electrolyte contacting the electrode [1]:

$$2H^{+}\ (aq) + 2e^{-} \rightarrow\ H^{2}\ (g) \tag{1}$$

The position of the $\varepsilon(H^{+}/H_2)$ level relative to the vacuum level on the energy scale has been calculated earlier using a Born–Haber thermochemical cycle [11]. Obviously, the electrons lose a part of their energy while migrating to a reaction center (**Figure 1**). And the top of the VB ought to be slightly below the oxidation energy level (**Figure 2**) at which hydroxyl groups are oxidized (−1.23 V, or −5.67 V, in compliance with the vacuum level):

$$\left(OH\right)^{-} + 2h^{+} \rightarrow H_2O + \frac{1}{2}O_2\left(g\right) \tag{2}$$

It should be also noted that the band structure imaged in **Figure 2** does not take into account the influence of the electrolytic environment to catalyst. When electrodes are put into water or aqueous electrolyte solution, the band levels and potentials can bend according to different scenarios, e.g., that suggested by Grätzel (**Figure 3**).

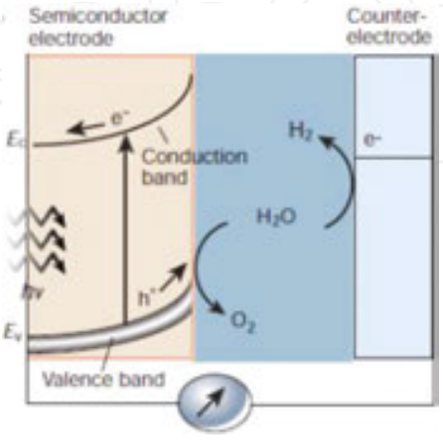

Figure 3. The band structure bending of *n*-type semiconductor in the presence of electrolyte [12].

http://dx.doi.org/10.5772/63236

Changes in the band potentials depend on charge surplus or shortage in the semiconductor. In other words, is it a *p*-type or *n*-type semiconductor? **Figure 3** illustrates *n*-type semiconductor, while for *p*-type direction of bending is opposite. Bending degree depends on several factors, e.g., on pH of electrolyte. Obviously, traditional first principle methods of *ab initio* simulations cannot describe the bending effect in principle and we do not consider it in this chapter. An important aspect of photocatalytic suitability is also a width of the band gap.

The energy threshold between SHE level and the level at which hydroxyl groups are oxidized is found to be 1.23 eV [1]. Taking the aforementioned requirements about the positions of the bands into account, it is easy to understand that the band gap width has to be larger than 1.23 eV (optimally, it should exceed 1.5 eV), which corresponds to ranges of visible light and near-infrared (IR) light. Also, the band gap must be narrower than 2.8 eV in order to allow a catalyst to employ energy of visible light and near-ultraviolet (UV) light, excluding UV range. UV light constitutes only few percents out of total Sun's irradiation (4–5% [4, 10, 13]), whereas the visible light constitutes 43–46% [13, 14]. Obviously, the band gap must correspond to the range of visible light in order to provide high efficiency of semiconductor photocatalysts.

Titania is considered to be prospective material for solving the problem due to a wide range of its properties [14]. Those include chemical stability, insolubility in water, nontoxicity, low price and sustainability against photocorrosion. Its position at the bottom of CB, formed by empty 3*d* atomic orbitals of titanium, is very beneficial – slightly above the SHE level, in respect to the requirement. However, the top of the VB, formed by 2*p* atomic orbitals of O atoms, is essentially below the level at which hydroxyl groups are oxidized. And the band gap is too wide – 3.2 eV in anatase- and brookite-structured phases, vs. 3.0 eV in rutile phase. In general, most metal oxides have band gaps larger than 3.0 eV [1].

Theoretical maximum of solar energy conversion degree for a titania catalyst with 3.2 eV wide band gap is approximately 1%. In turn, it is 15% for a catalyst with a 2.2 eV band gap (as for Fe_2O_3 bulk). A band gap of 2.0–2.2 eV width is generally considered to be optimum [15]. Still, according to another study, total energy losses are evaluated to be around 0.8 eV, which implies an optimal band gap of roughly 2.0 eV [16]. Photocatalytic water splitting efficiency must reach at least 10% conversion to be competitive against solar-cell-driven water electrolysis and to be economically profitable [15]. Obviously, photocatalytic properties of pristine TiO_2 bulk are not good enough to maintain the process effectively, so there is a need to modify the electronic structure of the material either by defect engineering (e.g., doping) or nanoscale transformation of its morphology. Our theoretical simulations show that pristine anatase-structured titania SWNTs rolled up from both (001) and (101) nanothin sheets possess the band gaps noticeably larger than those of TiO_2 bulk (by several tenths eV) [5, 7, 9]. On the other hand, the band gaps of doped titania NTs are essentially reduced, down to 2.2 eV in the case of N_O+S_O codoping of TiO_2 (001) NT [7].

2.2. Advances in experimental studies of TiO_2 photocatalysts

Numerous experiments focused on titania doping by different metal ions have already been performed. Among effective dopants one can find V, Ni, Cr, Mo, Fe, Sn, Mn and other cations [13]. In 1982, Borgarello et al. [17] discovered that Cr^{5+} doped TiO_2 could generate hydrogen

and oxygen in the process of water splitting under visible light irradiation (wavelength interval 400–550 nm). Klosek and Raftery [18] demonstrated that visible light absorption in titania doped with V^{4+} is a result of the electron transfer from the V 3*d* electron-induced energy level to the CB. Their research became a key to more effective ways of ethanol photooxidation under visible light, another route to hydrogen generation. Fe^{3+} doped TiO_2 also exhibits enhanced photocatalytic activity. Moreover, Fe^{3+} 3*d* electrons induce additional levels in the TiO_2 CB [19]. Doping of titania photocatalysts by Cr, Mg and Fe cations can improve their efficiency, for example, magnesium can reduce energy barrier for interphase transfer of electrons [20]. At the same time, the newly induced electronic states can behave as recombination centers, e.g., shift the impurity levels lower than the reduction SHE level.

TiO_2 doped by nonmetal ions exhibits a red shift of the absorption spectrum and possesses a higher photocatalytic activity than pure TiO_2, especially in the visible part of the solar irradiation spectrum [12]. Unlike metal ions, nonmetallic dopants usually do not induce new energy levels but squeeze the band gap directly by shifting the top of the VB upward [12], still it is not always the case. Nevertheless, Chen et al. [21] used X-ray photoelectron spectroscopy to show that in the electronic structure of C-, N- or S-doped TiO_2 the extra mid-gap states between the VB and the CB induced by dopants can appear. For example, titania doped by nitrogen exhibits high photocatalytic activity in water/methanol solution [22]. On the other hand, the S dopants substituting host oxygens or host titans can improve its photocatalytic activity too [23, 24]. Moreover, sulfur-doped titania exhibits higher photocatalytic activity with respect to the nitrogen-doped system [25]. The C-doped TiO_2 compounds were synthesized too [26], which exhibit a quite narrow forbidden gap and an enhanced photocatalytic activity than pure TiO_2 with mixed rutile and anatase domains. C-doped TiO_2 NTs also possess better photocatalytic activity [27]. Levels induced in the band gap were shown to broaden the activity of C-doped TiO_2 NTs from the visible to the IR region.

Limited amount of information on codoping of titania photocatalysts is available for nonmetallic dopants so far. Yan et al. [28] reported about the study on N- and S-codoping applied to TiO_2 NT array films by treatment with thiourea and calcination under vacuum and high temperature. The codoped NTs exhibit essentially broadened absorption spectrum and enhanced photocatalytic activity in methylene blue degradation process. Alternatively, Lv et al. [29] studied N+S codoped TiO_2/fly ash beads composite material and its photocatalytic activity in visible light range. Besides doped photocatalysts, appearance of vacancies as point defects can lead to rise in electrical conductivity and to changes in band gap structures [30].

2.3. Progress in *ab initio* modelling of TiO_2 photocatalytic efficiency

In spite of all the aforementioned efforts, the current understanding of fundamental changes in the electronic structure with atomic composition of doped semiconducting NTs is not sufficient for rational design of the atomic composition of these new compounds. To guide the search, a theoretical procedure is necessary in order to prudently predict the electronic structure and the charge redistribution in catalyst materials. Theoretical simulations performed up to date deal mainly with doped and codoped photocatalytic bulk materials [31–33], their low-index surfaces [34, 35] as well as nanoparticles and nanowires (NWs) [36, 37].

http://dx.doi.org/10.5772/63236

There are two critical issues that are important for photocatalysis but not yet well treated in the conventional density functional theory (DFT) and other packages: (a) the lack of resources, essential for simulations of the strong polarization on the charged electrode surfaces in aqueous electrolyte; (b) the inaccuracy of current DFT functionals in describing the redox levels of oxides (i.e., the band gap and positions of its edges relative to the H^+/H_2 and H_2O/O_2 levels) [38]. The great challenges still exist for the computation of photocatalytic reaction kinetics as it is driven by excess holes/electrons accumulated on the catalyst surfaces.

For titania bulk structure, spin-polarized DFT calculations predict that (2N, W) codoped TiO_2 can be considered as an efficient visible-light photocatalyst [31]. Using the projected augmented wave (PAW) method for *ab initio* calculations, Nolan found that small iron oxide clusters can be stable at the TiO_2 surface [34] and their presence squeeze the band gap towards the frequency range of visible light arising from the presence of iron oxide states lying above the VB of titania. The W-doped anatase (101) surface was also simulated using DFT PAW calculations [35]. C-, N- and S-doped $(TiO_2)_n$ nanoclusters were studied by Shevlin and Woodley using both DFT and time-dependent DFT calculations [36]. Asahi et al. [32] studied the band structure of the C-, N-, F-, P- and S-doped anatase structure of titania bulk using the same FP LAPW method. The substitution of O by N (which led to mixing of N(2*p*) and O(2*p*) states) produces the best conditions for photocatalytic applications since such structural modification results in upward shift of the top of the VB, thus reducing the width of the band gap.

A number of doped materials exhibit a large mismatch between the length scales over which the photon absorption takes place (up to micrometers), while at the relatively short distances within the limit of few tens nanometers, at which electrons can be extracted, electron–hole recombination was observed [16]. Reliable approach for solving this problem was found to be the synthesis of nanostructured electrodes with the orthogonalized directions of photon and electrons propagations, which is caused by markedly increased surface-to-volume ratios [39, 40]. Hollow NTs synthesized from the wide gap materials exhibit not only large surface area, but also high mechanical stability and integrity leading to both charge transport and electron–hole separation [41, 42]. TiO_2 (6,6) NTs built as regularly distributed bundles consisting of rutile (110) monolayers were calculated recently using DFT method [37]. Reported electronic structure of such a materials is predicted to be close to that of TiO_2 bulk. The electronic structures of the C, N, V and Cr doped as well as C/V, C/Cr, N/V and N/Cr codoped titania NWs were calculated too, in the case of C/Cr and C/V codoping a visible-light driven photoresponse was found to be the most enhanced [37].

On the whole, rather scarce number of publications focused on the computer simulations of defective NTs and NWs, including their photocatalytic properties, can be explained by a lack of methodical solutions for their construction in a variety of existing *ab initio* codes, which makes their comprehensive study very time-consuming and expensive. Meanwhile, the last versions of CRYSTAL code based on DFT-LCAO formalism, allow users either to exploit periodic rototranslation symmetry of 1D NTs, or to generate differently structured 1D NWs, setting the properly chosen Miller indexes of their lateral facets and simultaneously defining their crystallographic orientations, both for efficient ground-state calculations on their structural and electronic properties [43].

3. Theoretical background

3.1. Computational details

We have performed first-principle ground-state calculations on the SW anatase-structured TiO_2 (001) and (101) NTs, with fixed number of atomic layers as well as chiral indexes (n,0) vs. (−n,n), respectively, doped by C, N, S, or Fe atoms and codoped by pair of N and S atoms. We have simulated periodic and cluster models of doped NTs, for which either CRYSTAL code [43] or NWChem code [44] has been applied, respectively. For both types of DFT-LCAO calculations, we have used the formalism of the localized Gaussian-type functions (GTFs), which form the basis set (BS) of atomic orbitals for each chemical element as implemented in CRYSTAL and NWChem codes using crystalline and molecular orbitals constructed within either CO LCAO or MO LCAO approaches.

To avoid shortcomings of the traditional DFT methodology, especially underestimate of band gap widths, we have gone beyond this approach, applying the hybrid DFT-HF method for the electronic structure calculations. The hybrid functionals incorporate traditional Hartree-Fock (HF) approach determining the exchange energy E_x^{HF} [45]. Practical justification for this approach is the fact that errors of HF and DFT calculations often have opposite signs. For example, the former overestimates the values of band gaps while the latter underestimates them. The exchange-correlation energy in hybrid DFT-HF methods is expressed as linear combination of two quasi-independent contributions [43]:

$$E_{xc}^{DFT+HF} = \alpha_{DFT} E_{xc}^{DFT} + \alpha_{HF} E_x^{HF} \tag{3}$$

where coefficients determine hybrid functional parameters. It is very important to find such a functional which can be used for qualitative description of a large number of systems without additional parameters involved during calculation.

Values	α_{HF} = 14%	α_{HF} = 20%	Exp*
ε_{CB}, eV	−4.3	−4.2	−4.3
ε_{VB}, eV	−7.4	−7.8	−7.3
$\Delta\varepsilon$, eV	3.1	3.6	3.2

*Experimental values are taken from Ref. [4].

Table 1. Edges of the CB bottom (ε_{CB}), the VB top (ε_{VB}) and the band gaps ($\Delta\varepsilon$, eV) calculated for 20-layer TiO_2 (101) slab using the hybrid B3LYP functional vs. varied α_{HF}.

To perform all calculations on the pristine and doped titania NTs considered in this chapter, a modified B3LYP hybrid exchange-correlation functional [46] has been adopted by us since it provides the better reproduction for parameters of their atomic and electronic structure obtained earlier in experiments and theoretical simulations. To achieve a quantitative agree-

http://dx.doi.org/10.5772/63236

ment with the experimentally observed band gap for bulk anatase-structured TiO_2 ($\Delta\varepsilon$ = 3.18 eV) and the positions of band edges (**Table 1**), the admixture of nonlocal HF exchange in the B3LYP functional defined by α_{DFT} in Eq. (3) has been reduced from the standard 20% [43] to 14% [5].

The following configurations of localized GTF functions describing atoms of doped titania NTs are adopted by us for further first principle calculations:

(i) For Ti atoms in TiO_2, the basis set (BS) has been chosen in the form 411*sp*–311*d*, using the efficient core potentials (ECPs) implemented by Hay and Wadt [47].

(ii) Full-electron basis sets have been adopted for all other atoms, except Ti, which are contained in doped titania NTs, i.e., O: 8*s*–411*sp*–1*d*; C: 6*s*–411*sp*–11d; N: 6*s*–31*p*–1*d*, S: 8*s*–63111*sp*–11*d* and Fe: 8*s*–6411*sp*–41*d* [43].

The most comprehensive simulations have been performed by us for periodic models of NTs, for which the formalism of periodic rototranslation symmetry [43] has been exploited. This approach has been successfully applied by us earlier for simulations of perfect SW TiO_2 NTs of either anatase or fluorite phases [48, 49] as well as [001]- and [110]-oriented titania NWs of rutile phase [50, 51]. Reciprocal space integration over the direct and reciprocal lattices of NTs has been done by sampling the Brillouin zone of 2×2 supercells with 6×1×1 Pack–Monkhorst *k*-mesh [52] in order to ensure an equable summation over the direct and reciprocal lattices of NTs [45]. The outcome is 4 evenly distributed *k*-points within the segment of the irreducible Brillouin zone. Further increase of *k*-mesh results in much more expensive calculations yielding at the same time a negligible change in the total energy ($\sim 10^{-7}$ au). Self-consisted field calculations are considered as converged when the total energy differs by less than 10^{-7} au in two successive SCF cycles. For Fe- and N-doped NTs of both types as well as for the S+N codoped TiO_2 NT, spin-polarized calculations have been performed (as shown in Section 4.1 by the presence of doubly-generated DOS) since numbers of electrons per unit cell with opposite spins do not coincide, unlike pristine NTs and that doped by C and S atoms where these numbers are equal.

Hybrid DFT-HF calculations on cluster and periodic models of pristine and doped titania (001) NTs have been simultaneously performed by us using hybrid B3LYP functional as implemented in NWChem [44] and CRYSTAL [43] codes, respectively. Other computational parameters have been chosen similar in both codes. The obtained results have been comprehensively analyzed and compared [8]

3.2. Definition and verification of calculated properties

For reliable first-principle calculations of TiO_2 anatase-structured NTs, verification of bulk titania properties is a necessary step. Moreover, variation of α_{HF} when using B3LYP exchange-correlation functional has been performed as described in Section 3.1, to reproduce parameters of titania band structure with maximum precision (Table 1). Obviously, we have to check whether it is also true for structural parameters of anatase bulk crystal (**Figure 4**). Its lattice is characterized by tetragonal space group $I4_1/amd$ (space group Nr 141) [43, 49] with two formula units in the primitive cell. Two lattice parameters *a* and *c* measured experimentally (3.78 and

9.51 Å, respectively) are well correlated with those values calculated using hybrid DFT-LCAO B3LYP method (3.80 and 9.65 Å). Dimensionless parameter u of anatase lattice exactly reproduces its experimentally observed value (0.208 [45]). Thus, verification of obtained results gives us grounds to predict reliability of computational parameters for large-scale calculations on pristine and doped titania NTs possessing either (001) or (101) rectangular morphologies as well as (n,0) vs. (−n,n) chiralities, respectively.

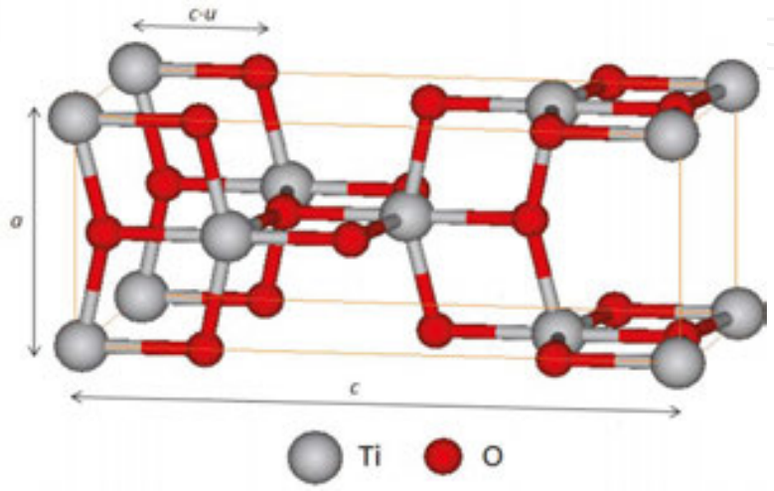

Figure 4. Unit cell of anatase-type titania lattice possessing tetragonal space symmetry.

To estimate the ability of forming single substitutional dopant in a substrate, e.g., NT, one has to calculate the corresponding formation energy:

$$E_{A_h}^{form} = E_{A_h/NT}^{tot} + E_h^{tot} - E_{A_h}^{tot} - E_{NT}^{tot} \tag{4}$$

where $E_{A_h/NT}^{tot}$ is the calculated total energy of a NT containing substitutional A_h atom, E_h^{tot} is the total energy of the host (h) atom, which is removed from the NT and $E_{A_h}^{tot}$ is the total energy calculated for the impurity atom while E_{NT}^{tot} stands for the total energy calculated for the perfect NT. Obviously, comparative analysis of formation energies for different dopants and sites of their location within various substrates allows one to determine energetically most favorable configurations of titania NTs for photocatalytic applications although conclusion on their suitability can be done when analyzing band structures.

Defective NTs are often characterized by the presence of defect levels inside the band gaps. In this case, the energy balance for possible water splitting under influence of visible light photons is changed. The differences between the highest occupied and lowest unoccupied impurity levels inside the band gap (HOIL and LUIL, respectively) are reduced in doped NTs, while preserving the proper disposition of these levels relatively to the redox potentials, so that [7]

http://dx.doi.org/10.5772/63236

$$\varepsilon_{VB} < \varepsilon_{HOIL} < \varepsilon_{O_2/H_2O} < \varepsilon_{H^+/H_2} < \varepsilon_{LUIL}\varepsilon_{CB} < \varepsilon_{CB} \quad (5)$$

thus, reducing the photon energy required for dissociation of H_2O molecule. Should a stand-alone electrode be unable to fulfill these requirements, other steps may be undertaken, e.g., application of external bias voltage or fabrication of a system consisting of two (or more) materials which are capable to ensure the required exciton generation as well as charge separation and migration when acting jointly. The redox potentials displayed in **Figure 2** are related to standard conditions and aqueous medium with pH = 0; further increase in pH value results in shifting both redox levels towards the vacuum level (**Figure 3**) [42].

3.3. Models and properties of (001) and (101) TiO_2 anatase slabs

Before folding of titania anatase-structured nanothin films to TiO_2 NTs, we have to understand their structure and main properties. **Figure 5** shows two slab models with the highest and lowest surface energy among anatase structures, i.e., (001) (0.90 J/m^2) and (101) (0.44 J/m^2), respectively [53].

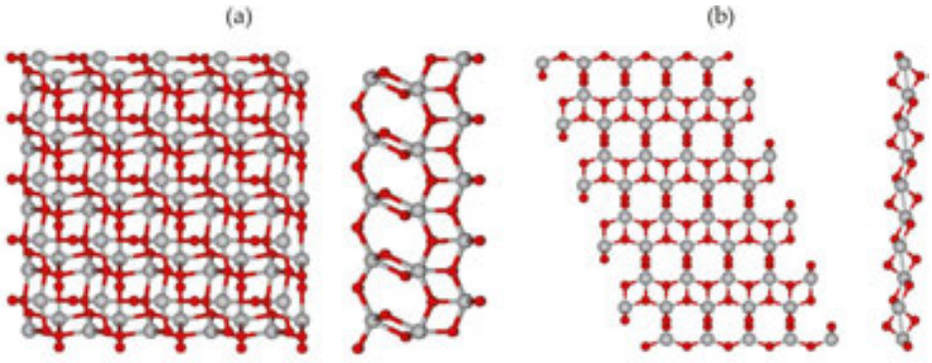

Figure 5. Atop and across views of 9-layer (001) (a) and 6-layer (101) (b) nanosheets of anatase-type titania [5]. Ti atoms are shown in gray, while O atoms are in red (dark gray) [5].

Obviously, (101) surfaces, normally the majority of the external surface of anatase titania (more than 94%, according to the Wulff's construction), are thermodynamically stable with a low surface energy, which determines its low reactivity [54]. On the contrary, (001) surface is characterized by the highest reactivity, e.g., towards adsorption of various species. To improve titania's reactivity, the preparation of shape-controlled TiO_2 nanocrystals with specific reactive facets exposed is a greatly desired, and the minority (001) surfaces with a higher surface energy attract extensive interest [55]. From the other side, an interesting effect was observed by Herman et al. who discovered reconstruction of (001) titania surface under ultrahigh-vacuum (UHV). This reconstruction significantly stabilizes the high-energy surface, but at the same time reduces its reactivity [56]. Therefore, investigation of possible facet reconstruction is important, and developing novel synthesis routes is necessary to prevent the reconstruction. Reactivity of the NTs under consideration is another important aspect.

3.4. Models of pristine and doped titania NTs

First, we have studied photocatalytic efficiency of pristine anatase (001) NTs (**Figure 6**) folded from 9-layer (001) slab (**Figure 5**). Range of NT diameters has been varied from 0.6 to 4.0 nm [5]. Optimized model of TiO_2 NT (**Figure 6**) has been used for simulation of different properties as described in Section 4.1 (formation energies, widths of band gaps and positions of their edges at the top of the VB and the bottom of the CB as well as mid-gap levels induced by dopants).

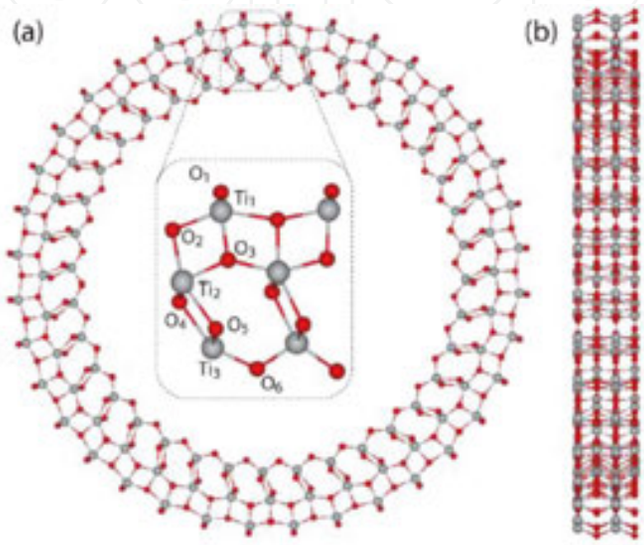

Figure 6. Schematic images of a unit cell monoperiodically repeated along a (36,0) TiO_2 (001) NT (d_{NT}=4.81 nm) having the substitutional point defects: (a) nanotube's top view; (b) nanotube's side view. Ti atoms are shown in gray, while O atoms are in red (dark gray). At the inset drawn in (a) the basic unit cell of the TiO_2 NT is repeated by 18 symmetry rototranslational operators. The numbered titan and oxygen atoms of the inset show the substitutional sites for impurity defect atoms (A_h, where "h" is for "host" atom) [7].

We have chosen the 2×2 supercell of the (001) nanosheet prototype (**Figure 5a**), when constructing pristine 9-layer TiO_2 (36,0) NT with an internal diameter of 3.47 nm and walls of thickness 0.67 nm (**Figure 6**) for further doping. Such a NT contains 648 atoms per NT unit cell. In our study, C, N and S impurities substitute the host oxygens in six possible positions (shown in the inset of **Figure 6**), while three possible dopant positions have been considered for Fe_{Ti} substitute. We define the defect concentration as the number of dopant atoms relative to the number of atoms per supercell of a periodic structure which can be substituted by the dopant. Since the extended periodically repeated 2×2 supercell possesses 12 TiO_2 formula units, incorporation of the doping impurity leads to the 8% defect concentration in the titania NT for the Ti site and ~4% for the O site. Modelling nitrogen and sulfur codoping at the titania NT with similar defect concentration, we have substituted oxygens in O_1 and O_2 sites by S- and N-dopants as shown in **Figure 6**. We note that reduction of defect concentration results in larger supercell and leads to expensive calculations beyond our current computer facilities. For the same reason, charge compensation defects for anionic dopants are not considered in this study at all.

http://dx.doi.org/10.5772/63236

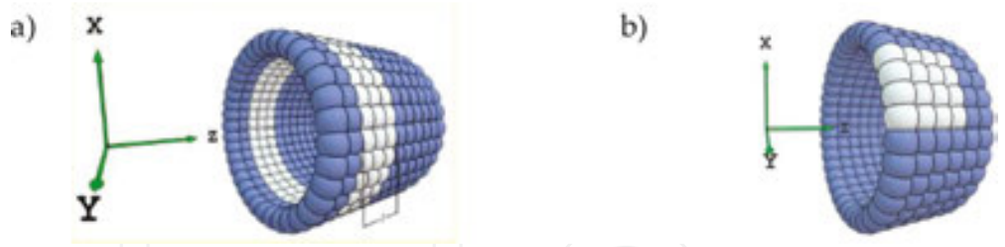

Figure 7. Cluster models of TiO_2 (001) NTs: (a) ring fragment and (b) arc segment of ring.

For cluster models of TiO_2 (001) NTs, we use either several rings cut from periodic NT models (**Figure 7a**), lengths of which correspond to the period of 1D NT, or even arc fragments of rings (**Figure 7b**), which can be transformed to the whole rings using rototranslational symmetry. Important part of cluster models is their boundary conditions around broken edges which substitute the absence of periodicity in 0D models by hydrogen atom termination of all broken bonds [8].

Initial internal morphology of cluster corresponds to analogous NT structure. Cluster models have been used for simulation of (001)-oriented TiO_2 NTs only. In Section 4.2, we perform comparative analysis of photocatalytic properties of doped anatase-structured NTs obtained in cluster and periodic models.

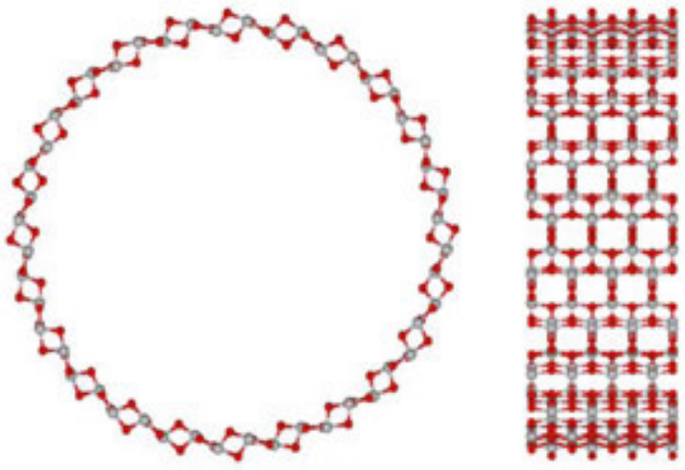

Figure 8. 6-layer TiO2(101) NT with chirality indexes (−12,12): front view (left panel) and aside view (right panel). Large Ti atoms are shown in gray, while O atoms are in red [9].

A number of pristine 6-layered anatase (101) NTs with chirality indexes (n,n) and (−n,n) have been modelled. TiO_2 (101) NT with chirality indexes (−12,12) has been chosen (**Figure 8**) as optimal for further doping. This choice is a result of compromise between the minimal formation energy estimated according to Eq. (4) and a number of atoms in the NT unit cell. Such a NT consists of 432 atoms per unit cell. Here, we consider NTs 1×3 and 2×3 periodically repeated "basic" unit cells containing 36 and 72 atoms, respectively, giving dopant concentration of 2.78% (12 dopant atoms per NT unit cell) and 1.39% (6 dopant atoms per NT unit

cell), respectively. Suitability of these (101) titania NTs for photocatalytic applications is discussed in Section 4.3.

4. Photocatalytic efficiency of doped titania NTs

4.1. Periodic model of doped (001)-oriented NTs

The energy balance between the band gap edges (e.g., mid-gap levels induced by defects) and the redox levels described in Eq. (5) is considered as a criterion for efficiency of photocatalytic water splitting [1, 4, 38]. **Figure 9** includes a pair of vertical lines denoting the reduction and oxidation levels fixed in the plots of the densities of states calculated for pristine and doped TiO_2 NTs. The band gap edges of the titania anatase-structured (101) slabs are compared with the corresponding experimental values presented in Table 1 (Section 3.1).

We note that the band gap edge positions presented in Table 1 differ not more than 0.1–0.2 eV from those experimentally observed, which gives us a reason to believe that predictions made by us on the electronic structure of doped TiO_2 NTs are at least qualitatively and possibly semiquantitatively reliable.

n	C_{On}	N_{On}	S_{On}	Fe_{Tin}
1	**1.16****	3.79	**2.61****	5.58
2	3.23	**3.56****	3.6	5.42
3	2.99	3.95	4.34	**5.37****
4	3.13	3.88	5.33	–
5	3.31	4.08	5.65	–
6	3.78	4.11	3.37	–
Bulk***	4.12	3.22	5.36	4.44

*Host atoms A_h substituted by impurities (h) are labeled in **Figure 8**.
**The lowest formation energies for each dopant are shown in bold.
***The last row contains $E_{A_h}^{form}$ values calculated for doped anatase bulk using 2×2 supercell.

Table 2. Defect formation energies ($E_{A_h}^{form}$, eV) in doped TiO_2 NTs calculated using Eq. (4)*. *n* is index number of $O_{(n)}$ or $Ti_{(n)}$ atoms imaged in **Figure 6** (inset).

In our study, impurity atoms have substituted each possible irreducible host O or Ti atom in the NTs with rototranslationally and periodically repeated cells as shown in **Figure 6** (Section 3.4). Therefore, one of the six types of O atoms and one of the three types of Ti atoms have

http://dx.doi.org/10.5772/63236

been consequently substituted by C_O, N_O, S_O and Fe_{Ti}. According to our calculations, the carbon and sulfur dopants would prefer to be positioned at the site of the outermost oxygen, while nitrogen would prefer the second oxygen layer counting from the outer side (**Table 2**).

Obviously, the smallest formation energy of anion dopants has been found for C_O (1.16 eV). For S_O-doped TiO_2NT, $E_{A_n}^{form}$ = 2.61 eV, while 3.56 eV is required for N_O dopant. The most energetically favorable position for the host Ti atom to be substituted by iron atom ($E_{A_n}^{form}$ = 5.37 eV) to be located in the Ti layer closest to the inner wall of the titania NT (inset of **Figure 6** and Table 2). When calculating the band structure of the doped NTs, only the NTs with the smallest defect formation energies have been taken into account. The formation energy of the nitrogen–sulfur pair has been obtained to be 5.64 eV, which fulfils the relation $2E^{form}(S_O) < E^{form}(S_O+N_O) < 2E^{form}(N_O)$ (in accordance with Table 2), thus confirming the approximate additivity of estimated dopant formation energies, when these contain different numbers of impurity atoms, irrespective of their chemical nature. Substitutional point defects in TiO_2 NTs reveal a tendency to form defect-induced levels inside the optical band gap. In the case of the C_{O_1}/TiO_2 NT, the filled band is positioned ~2.2 eV above the top of the VB (**Figure 9b**), while in the case of the N_{O_2}/TiO_2 NT impurity (**Figure 9c**), the induced mid-gap state is found to be 0.9 eV above the top of the VB. The mid-gap states computed for the S_{O_1}/TiO_2 NT (**Figure 9d**) forms the top of the VB (for the S-doped bulk, the defect level lies ~0.2 eV above the top of the VB), and in the case of Fe_{Ti_3}/TiO_2 NT, the vacancy-induced level is positioned in the middle of the band gap (**Figure 9f**). The top of the VB of the perfect titania NT is formed by O 2*p* orbitals, while the bottom of the CB is formed by Ti 3*d* states.

The projected DOS computed for the nitrogen and sulfur codoped TiO_2 NT is shown in **Figure 9e**. For the nitrogen and sulfur codoped TiO_2 NT, the N-dominated mid-gap levels shift by 0.3 eV downward, formed the occupied gap level below the O_2/H_2O redox potential. By the presence of the sulfur codopant, the bottom of the CB shifts downward with an energy gap of about 2.2 eV, thus reducing the photon energy required for water splitting reaction. The nitrogen and sulfur codoped structure exhibits a gap state below the top of the VB because of defect–defect interactions. For this system the top of the VB and the bottom of the CB shift downward relative to the nitrogen-doped structure. Relative to the bottom of the CB of the sulfur-doped structure, the CB shifts back toward the CB position of the pristine structure. Codoping thus gives rise to visible-light-driven excitation from the mid-gap states of 2.3 eV, which is just slightly smaller than for the nitrogen-doped NT. This allows one to predict that nitrogen and sulfur codoped TiO_2 NTs can be suggested as a good candidate for the visible-light-driven photocatalytic water splitting [30].

On the basis of the standard thermodynamic conditions of an active photocatalyst for H_2O splitting, we discuss and evaluate the influence of the incorporated cation and anion species on the photocatalytic activity of TiO_2 NTs. We have calculated the total and projected DOS for C-, N-, S- and Fe-doped NTs, as compared with that of pristine TiO_2 NT (**Figure 9**). The schematic representation of the band gap edges and mid-gap states of all these NTs is shown in **Figure 10**.

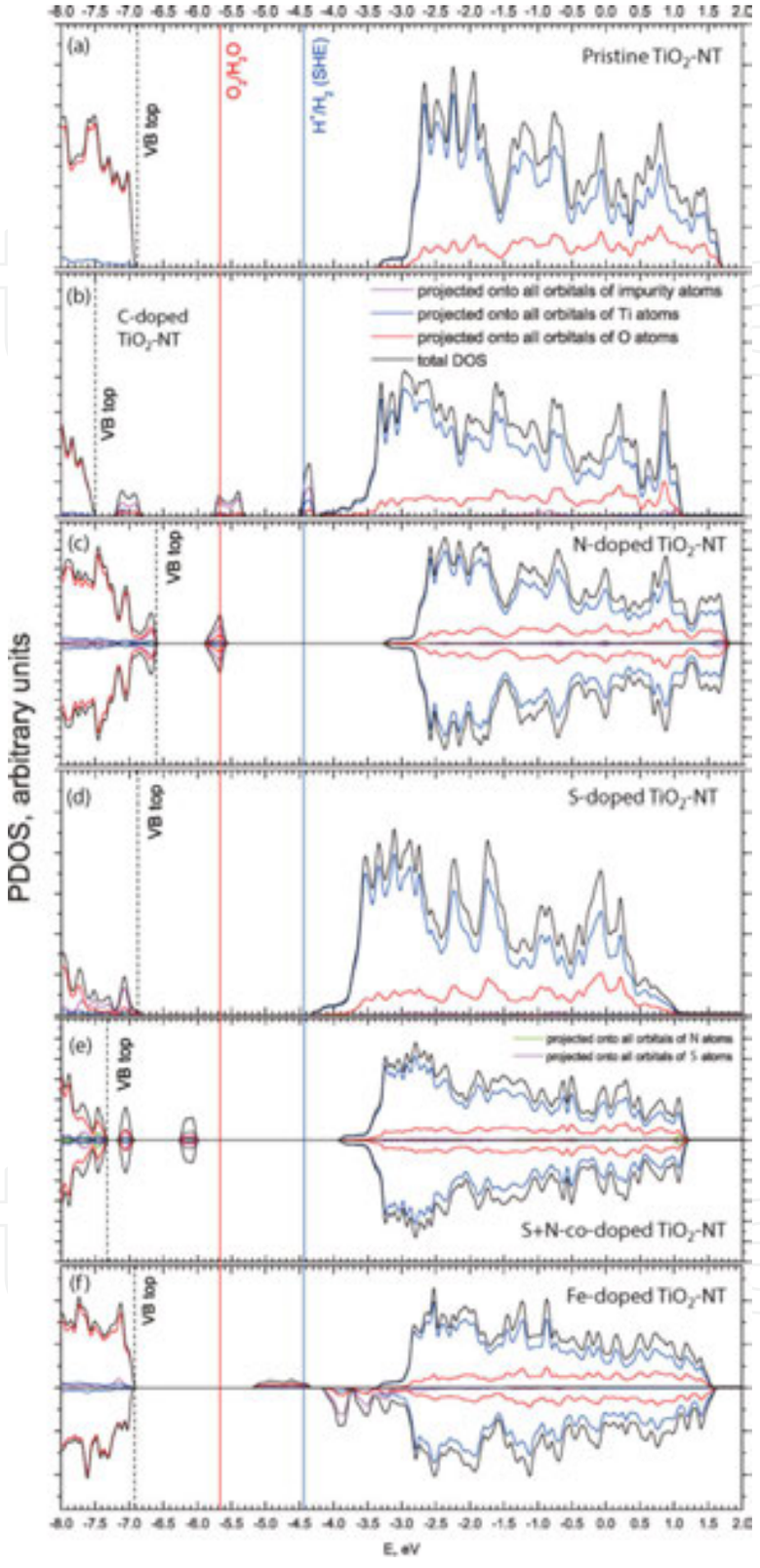

Figure 9. Total and projected densities of states calculated for perfect and doped titania nanotubes: (a) pristine, (b) C-doped, (c) N-doped, (d) S-doped, (e) N+S codoped and (f) Fe-doped. Vertical lines stand for ε_{O_2/H_2O} and $\varepsilon_{H^+/H2}$ potentials. Zero of the energy scale corresponds to the vacuum level [7].

http://dx.doi.org/10.5772/63236

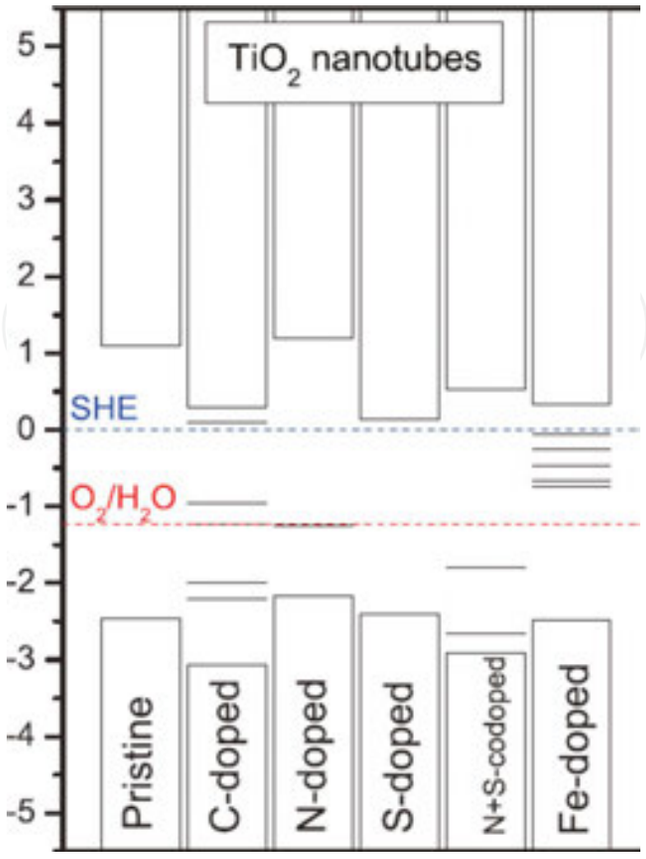

Figure 10. Schematic representation of the band edges and mid-gap states of pristine and doped TiO_2 nanotubes. The blue and red horizontal dashed lines correspond to the redox ε_{O_2/H_2O} and ε_{H^+/H_2} potentials, respectively. Zero of the energy scale corresponds to the standard hydrogen electrode (SHE) [7].

As can be seen from Table 2, the most energetically favorable positions for anion dopant on titania NT are the outer host oxygen atoms, while Fe prefers to substitute the inner titan atoms. For pristine TiO_2 (001) NT, the bottom of the CB is ~1.0 eV above the H^+/H_2 potential, whereas the top of its VB is ~1.2 eV below the O_2/H_2O potential (**Figures 9a** and 10). A carbon substitutional impurity in a TiO_2 NT induces an occupied defect level ~0.2 eV above the oxidation potential (**Figures 9b** and **10**). This leads to an unsuitable VB position for the oxygen evolution reaction. The N-doped TiO_2 NT possesses an occupied impurity level practically at the O_2/H_2O potential (**Figures 9c** and **10**), while the bottom of the CB relative to the perfect NT is almost unchanged. For the sulfur-doped titania NT, we predict that the bottom of the CB is located almost at the level of reduction potential, while the top of the VB corresponds to that of the ideal NT being practically unchanged (**Figures 9d** and **10**). The iron-doped titania NT exhibits defect-induced mid-gap states about 0.5 eV lower than the ε_{H^+/H_2} level (**Figures 9f** and **10**), which results in the recombination of electrons and holes. On the whole, considering the possible configurations of the doped titania NT, we predict that the most efficient nanophotocatalyst for the visible-light-driven H_2O splitting could be N and S codoped titania NTs (cf. **Figures 9e** and **10**).

4.2. Cluster models of doped (001)-oriented NTs

To verify the periodic model of doped SW nine-layer (36,0) TiO_2 (001) NT (**Figure 6**) and results obtained in its DFT-LCAO calculations, we have performed time-dependent TD DFT-LCAO calculations, using NWChem code [44], on 2×2, 3×3 and 4x4 arc-segment models of TiO_2 NT (**Figure 7**), reproducing the morphology of periodic NT and providing adequate boundary conditions around each cluster model as shortly described in Section 3.4 [8]. Positions of N_O and S_O (as the most preferable dopants) are also reproduced from the periodic model of doped titania NT (**Figure 6**).

To perform simultaneously 1D NT and 0D cluster calculations within the same theoretical approach described in Section 3.1, we have used a modified B3LYP hybrid exchange-correlation functional [46] adopted earlier to perform periodic calculations on the doped titania NTs [5–7].

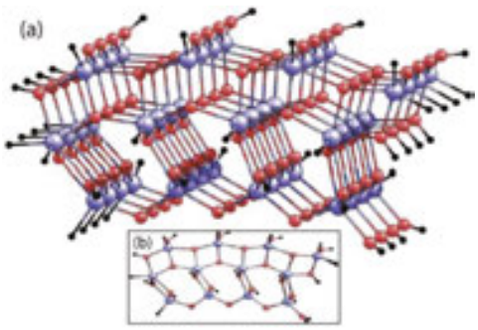

Figure 11. (a) Schematic representation of the 0D 4 × 4 fragment of TiO_2 NT (chosen as its cluster model) with dangling bonds saturated by hydrogen atoms (black). (b) Front view [8].

We have studied 0D cluster models of the 1D periodic NTs intending to perform TD-DFT calculations, which unfortunately are still not possible using the periodic first principle codes. Meanwhile, it is possible to run these calculations within cluster approach, e.g., using NWChem code [44]. On the other hand, this code does not admit performance of periodic 1D calculations, which also should take into account the symmetry of system allowing growth of size for model with correspondingly arranged atoms. To reduce the total number of atoms, while preserving geometry and stoichiometry, we have generated a number of 0D clusters by slicing the NT (**Figure 11**). Since it is possible to perform both 1D and 0D calculations at the same level of theory with the same set of parameters, the results calculated for the 1D NTs can serve as a performance benchmark for the 0D cluster models. We have sliced the NT into different arc-segments $n \times n \times d$ (**Figure 7**), where d is the NT's thickness (a constant, and therefore omitted from the clusters' shorthand notation $n \times n$), while n has been chosen to be 2, 3 and 4. During calculations, positions of atoms in clusters have been kept fixed to avoid relaxation and to preserve the curvature of the NT.

We have simulated stoichiometric segment-like 0D clusters with varying parameter n and with different terminations of the bonds that were broken while cutting the NT. In such models, a common practice is to saturate broken bonds with hydrogen atoms [57]. However, in order to

http://dx.doi.org/10.5772/63236

reproduce a partial charge on the outermost Ti atoms, we explored several saturation modes other than H. Hydrogen is less electronegative than oxygen, and when slicing the NT, we disconnect titanium from oxygen and pair Ti with H, effectively altering metal's partial charge. To compensate for that, we have tried also to terminate our clusters with hydroxyl groups OH and with halogens F and Cl. However, our results indicate that these substituents not only introduce a number of electronic levels, polluting the gap between the highest occupied molecular orbital and the lowest unoccupied molecular orbital (HOMO/LUMO), but they also shift the energies of these orbitals by 1–2 eV. Hydrogens do that as well (**Figure 12**), but their effect on the HOMO/LUMO energies is less pronounced.

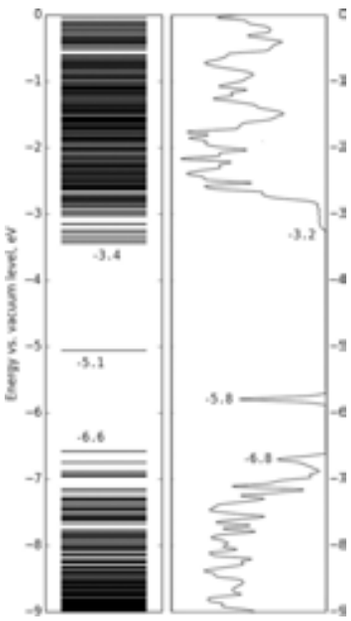

Figure 12. Left: MO levels of the 4 × 4 0D cluster model for the N-doped TiO_2 NT. Right: The total density of states for the 1D NT model of the analogous N-doped titania nanotube [8].

Arrangement of H-saturated atoms is another important issue. A change between relaxed and unrelaxed geometry (effectively, a difference of ca. 0.1 Å in Ti–H bond length) translates into 0.5 eV large shift of the band edges. We have achieved the best agreement between 0D and 1D models (in terms of band edges' energies and HOMO/LUMO energies, respectively) for H-terminated 0D clusters. Coordinates of terminating atoms in them have been relaxed relative to the TiO_2 backbone (which has been kept rigid during the optimization to preserve the geometry of the NT). To sum up, in all our calculations that we shall discuss further, clusters are arc-segments of the NT, that preserve stoichiometry and curvature of the NT, with any dangling bonds saturated by hydrogen atoms. Positions of these atoms relative to fixed coordinates of Ti and O atoms are relaxed in order to minimize the total energy of the object. To avoid a gap pollution, we have decided not to analyze any states dominated by energies arising due to hydrogen atoms. We have achieved this by excluding all the states in which hydrogen orbitals contribute to the electron density more than 2.25%.

The 0D cluster models have been investigated with the goal of using NWChem's implementation of the TD-DFT method [44] to perform nonadiabatic simulations of the relaxation on both NT and its environment following absorption of a photon. For direct verification of cluster calculations using results obtained for periodic NT, we have considered 4×4 cluster model of N-doped TiO_2 (001) NT (**Figure 11**). However, due to size restrictions, this model does not allow us to simulate N+S codoped NT. To compare with results of periodic model calculations, we construct MO level distribution in cluster models vs. total DOS for TiO_2 NT (**Figure 12**) as well as schematic representation of the band edges and mid-gap states of pristine and doped TiO_2 NTs imaged for periodic and three cluster models: 2×2, 3×3 and 4x4, where the extension numbers denote the number of elementary cells along and perpendicular to the NT axis, respectively (**Figure 13**). Within our notation, the top of the VB and the bottom of the CB have been defined as, respectively, the highest occupied level and the lowest unoccupied level the contribution to which from dopant atom orbitals is relatively small. **Figure 13** displays the band edges within this set of definitions. It also shows a converging trend: while for the undoped 2×2 clusters the disagreement with the pristine 1D NT model is quite noticeable, while it becomes less significant for the 3×3 clusters and even more so for the 4×4 clusters. Unsurprisingly, 0D models reproduce the top of the VB more accurately than the bottom of the CB. What is surprising is that the relative positions of the defect-induced mid-gap states with respect to the band edges between the 1D and 0D models are similar, even though they possess very different defect concentrations. For example, the left side of **Figure 12** shows the single level at the gap between the LUMO and HOMO levels which is dominantly composed of N $2p_x$ states (along the NT axis). The band edges of 0D and 1D models become closer while the 0D cluster size increases, yet the position of the defect-level does not show any convergence. At −5.1 eV, it is significantly higher for the 4×4 0D cluster than the value of −5.8 eV for the 1D NT.

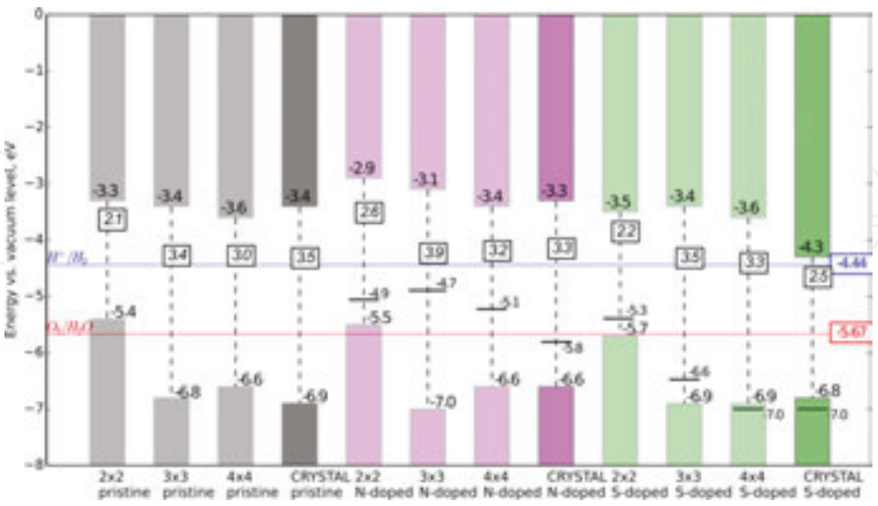

Figure 13. Comparison of band edges and gaps obtained for 0D and 1D NT models. All values are given in terms of electron volt vs. vacuum level; ε_{H^+/H_2} and ε_{O_2/H_2O} potentials are given for reference. CRYSTAL data refer to 1D models while 0D results are obtained using NWChem code [8].

http://dx.doi.org/10.5772/63236

Noncoincidence of the dopant-induced levels in both 0D and 1D NT models may be a consequence of the effectively larger defect concentration in the latter, which is 1 dopant per 24 O atoms in the periodically repeated unit cell (≈4%), versus 1 dopant per 96 O atoms (≈1%) in the 4×4 0D cluster. For S-doping, size of the cluster heavily affects position of the defect level. Moreover, for 2×2 and 3×3 models, the positions of S-induced levels are qualitatively different from those of 4×4 and NT models: the former are in-gap while the latter are located below the top of the VB.

To conclude, we observe that the 0D model qualitatively corresponds to the 1D model as far as the band edges are concerned. Positions of the dopant-induced states, however, strongly depend on the size of the cluster and, therefore, differ from those calculated for the NT. In N-doped cluster, where this effect is the most emphasized, it can be partially attributed to the spin polarization of the system, although the relatively naïve definition of the cluster model could have affected it just as much. More elaborate schemes exist, for example, polarizable polar background embedding [58], but these schemes are beyond the scope of our study.

4.3. Periodic models of doped (101)-oriented NTs

For energetically more stable but possessing lower reactivity (101) types of TiO_2 NTs with anatase morphology, we have considered only N and S dopants as well as N+S codoping since C- and Fe-substitutes have been found to be ineffective for photocatalytic applications of (001)-oriented TiO_2 NTs (Section 4.1). Calculations on these NTs have been performed using the same DFT-LCAO method with the hybrid exchange-correlation functional B3LYP [46] as used earlier having 14% of nonlocal Fock exchange as implemented in CRYSTAL code [43].

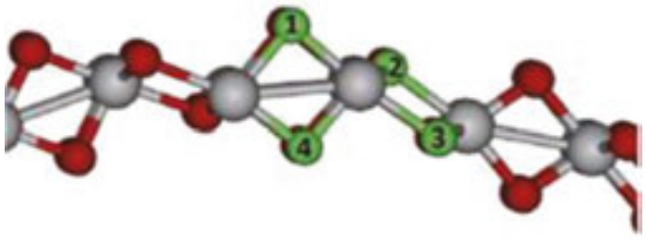

Figure 14. Nonequivalent S or N dopant positions in the segment of 6-layer wall of (−12,12) TiO_2 (101) nanotube (**Figure 4**) [9].

As mentioned in Section 3.4, the pristine titania NT with chirality indexes (−12,12) (**Figure 8**) has been chosen as the most suitable for our simulations on the doped TiO_2 (101) NTs. We consider four possible dopant sites to substitute the nonequivalent oxygen atoms (**Figure 14**). We denote the outermost O site as position 1, while the innermost O site is position 4. The S1 site is found to be the most energetically favorable – it requires the lowest formation energy per unit cell/dopant, 2.47 eV for both concentrations (**Table 3**). As it has been found in all cases the S dopant shows a tendency to be displaced from its initial position. The displacement direction is orthogonal to the tangent line passing through the initial S atom position, and the S atom is protruding out the NT wall. Obviously, it is easier to follow such displacement from

initial positions S1 and S4, which explains that the dopant formation energies are lower for these cases. Formation energies of S dopants presented in **Table 3** almost do not depend on their concentration, unlike N dopants for which this dependence is noticeable, excluding external N1 site.

	Concentration of defects			
Site	1.39%		2.78%	
	S_O	N_O	S_O	N_O
1	**2.47***	**3.39***	**2.47***	**3.39***
2	2.89	3.49	2.90	4.10
3	3.43	3.51	3.47	4.15
4	2.62	3.51	2.62	3.39

*The lowest energies are shown in bold.

Table 3. Defect formation energy (in eV) of S and N dopants at 2.78% and 1.39% defect concentrations as calculated using Eq. (4).

For the two sulfur dopant sites lying closer to the outer surface, sites S1 and S2 (**Figure 14**), there is a negative shift in energy for both the bottom of CB and the top of the VB. In fact, there is no difference between CB/VB positions of the pristine NT and the NTs containing S dopants at the positions S3 and S4. Doping at positions S1 and S4 promotes the highest photocatalytic enhancement, reducing the gap between the lowest unoccupied state and the highest occupied state, from 4.19 eV to 3.14 eV (3.12 eV) vs. 3.08 eV (3.07 eV) for 1.39% (2.78%) defect concentrations, respectively. It means that sulfur atoms themselves do not provide sufficient rise of photocatalytic activity. S-induced occupied levels have been found to be lower at 1.39% concentration. Unlike S-doped NTs, N dopants do not induce any visible shift in positions of the VB top and the CB bottom, levels are almost the same as in the case of the pristine structure. N dopants, however, induce empty states inside the band gap. For 2.78% defect concentration these empty states are not always higher than the highest occupied state. For N2 case, the empty state is located below an occupied state and is very close to the VB top, which means that in reality it will be easily occupied by electrons with similar energies.

Suitability of N_O+S_O codoped TiO_2 (101) NTs is likely noticeably higher than S and N monodoped ones. Indeed, in the latter, there are only four nonequivalent dopant positions (**Figure 14**). However, after one dopant is already introduced, a number of options for different combinations of codopant positions appear. Due to limited computational resources, we have decided to put S dopant in its preferable position, S1 (**Figure 14** and Table 3). Therefore, in every modelled codoped structure the S atom is fixed in position 1, while N dopants can be inserted in different surrounding positions. Possible dimer-type sites for S+N codopants are assigned by additional indexes for identification (**Figure 15**: "*FR*" stands for "front", "*B*" for "between", "*N*" for "near" and "*UND*" for "under").

http://dx.doi.org/10.5772/63236

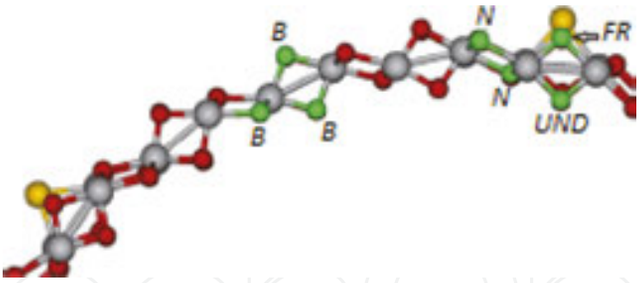

Figure 15. Possible sites for N dopant if S atom is located in position S1 (**Figure 14**), in the segment of 6-layer wall of (−12,12) TiO_2 (101) nanotube [9].

Electronic diagram of six studied N_O+S_O codoped TiO_2 NT configurations with defect concentration of 2.78% is shown in **Figure 16**. Obviously, (N3-S1)*B* and (N3-S1)*N* are identical (**Figure 15**), and one of them (the latter) must be excluded from further consideration. The general observation is that the enhancement of the photocatalytical efficiency of the simulated structures may be expected. In four cases out of six, the lowest empty state is induced slightly below the ε_{O_2/H_2O} level (oxygen potential), and the highest occupied state is located between the empty state and the VB top. The distances between the empty and the occupied induced states are the smallest for $(N1\text{-}S1)_B$ or $(N4\text{-}S1)_B$ configurations, which means that it might be relatively easy for electrons to transfer to the empty state and, consequently, to overcome the $\varepsilon_{H^+/H_2} - \varepsilon_{O_2/H_2O}$ interval between redox potentials (**Figure 16**). The general observation is that in most cases S and N atoms have a tendency to be found closer to each other.

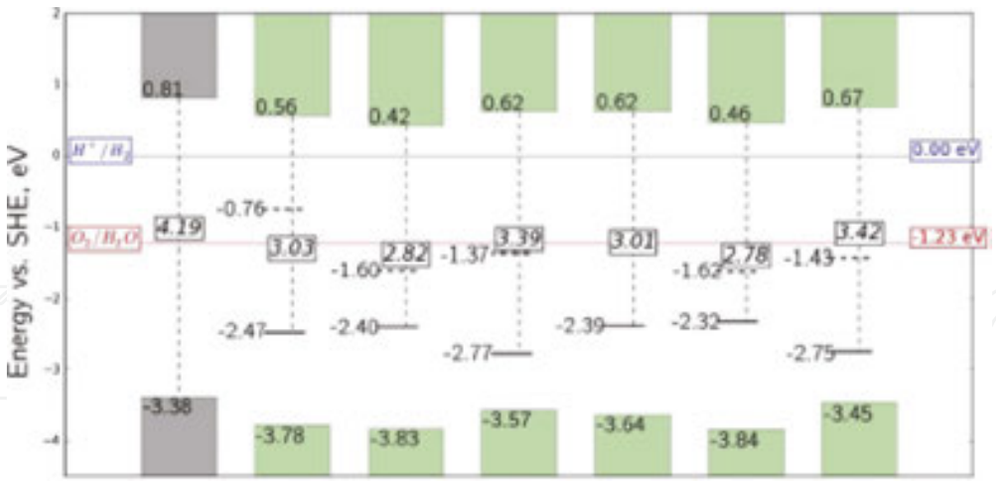

Figure 16. Energy diagram for the band gap edges and mid-gap states of pristine and N+S codoped TiO_2(101) NTs. Gray column correspond to pristine (−12,12) NTs while green columns from the second to the sixth from the left correspond to (N1-S1)*FR*, (N1-S1)*B*, (N2-S1)*N*, (N3-S1)*B*, (N4-S1)*B* and (N4-S1)*UND* codopants imaged in **Figures 14** and **15** [9].

Based on the results of our calculations, we predict that S or N dopants alone introduced into the 6-layer TiO_2 (−12,12) NT cannot result in a significant rise of photocatalytic response. For instance, the N doping may induce empty mid-gap states that can disrupt the photocatalytic

process. We found that defect concentration does not have a big impact on the electronic structure of NTs under study; our results show that rise in defect concentration from 1.39% to 2.78% (of doping atoms per unit cell) practically does not shift the band gap edges and mid-gap states induced by these defects. We show that the S+N codoping of titania NT can result in enhancement of photocatalytic efficiency, at least qualitatively. At the same time, we have to conclude that changes of titania NT electronic structure induced by codoping depend on defect concentration.

5. Summary

1. In a series of recent papers [5–9], we have formulated main goals of our studies:

   a. To evaluate photocatalytic suitability of inorganic nanostructures, as a first step we have considered SW titania anatase-structured (101) and (001) NTs, both pristine and doped.

   b. To justify application of computational methods of ground state *ab initio* DFT-LCAO calculations, e.g., CRYSTAL code (periodic structures of different dimensionalities) and TD DFT NWChem code (0D cluster structures), reliability of both models as well as reliable choice of hybrid Hamiltonian.

   c. To calculate the structural and electronic properties of nanomaterials under study in order to estimate their mechanical durability and homogeneity, electronic structure and photocatalytic efficiency.

   d. To search for novel nanomaterials suitable for photocatalytic applications.

2. Main results obtained in our large-scale computer simulations:

   a. Both SW (001) and (101) titania NTs are suitable for photocatalytic applications: although the latter is more stable energetically, the former possesses noticeably higher chemical reactivity.

   b. The necessary condition to achieve suitability of doped nanostructures for photocatalytic application is a proper disposition of band gap edges and impurity levels relative to the redox potentials: $\varepsilon_{VB} < \varepsilon_{HOIL} < \varepsilon_{O_2/H_2O} < \varepsilon_{H^+/H_2} < \varepsilon_{LUIL} < \varepsilon_{CB}$ where HOIL and LUIL are the highest occupied and the lowest unoccupied impurity levels, respectively.

   c. The next condition for such a suitability is the absence of the impurity levels between oxidation and reduction levels ε_{O_2/H_2O} and ε_{H^+/H_2}, respectively, in order to exclude electron–hole recombination.

   d. The best candidates for doping of titania NTs have been found to be N_O and S_O substitutes, however, N_O+S_O codoping of TiO_2 NTs is certainly the best choice.

3. Further activities in the field of theoretical simulations in order to evaluate photocatalytic suitability of nanoelectrodes:

   a. To look for the best nanomaterials, both NTs and NWs, we have already studied $SrTiO_3$ NWs [59] and continue comprehensive simulations on ZnO NWs including their doping.

   b. To look for new types of defective structures of studied nanomaterials suitable for photocatalytic applications, e.g., vacancies and cation dopants.

   c. For better understanding of photocatalytic processes upon nanoelectrodes we are beginning TD DFT calculations on their charged and excited states.

   d. To study the charge transfer at the surface of doped nanoelectrodes immersed in aqueous electrolyte we intend to perform large-scale nonadiabatic molecular dynamics (MD) calculations.

This study has been supported by the EC project WATERSPLIT (ERA.Net RUS Plus project No. 237). The authors are indebted to A.V. Bandura, P.N. D'yachkov, R.A. Evarestov, E. Spohr and M. Wessel for stimulating discussions.

Author details

Yuri F. Zhukovskii*, Sergey Piskunov, Oleg Lisovski, Andrei Chesnokov and Dmitry Bocharov

*Address all correspondence to: quantzh@latnet.lv

Institute of Solid State Physics, University of Latvia, Riga, Latvia

References

[1] C.R.A. Catlow, Z.X. Guo, M. Miskufova, S.A. Shevlin, A.G.H. Smith, A.A. Sokol, A. Walsh, D.J. Wilson, and S.M. Woodley. Advances in computational studies of energy materials. Philos. Trans. Royal Soc. A, 2010, 368, p. 3379–3456.

[2] M. Kitano and M. Hara. Heterogeneous photocatalytic cleavage of water. J. Mater. Chem., 2010, 20, p. 627–641.

[3] N.S. Lewis. Toward cost-effective solar energy use. Science, 2007, 315, p. 798–801.

[4] A. Kudo and Y. Miseki. Heterogeneous photocatalyst materials for water splitting. Chem. Soc. Rev., 2009, 38, p. 253–278.

[5] O. Lisovski, S. Piskunov, Yu.F. Zhukovskii, and J. Ozolins. *Ab initio* modeling of sulphur doped TiO_2 nanotubular photocatalyst for water-splitting hydrogen generation. IOP Conf. Ser.: Mater. Sci. Eng., 2012, 38, 012057 (p. 1–5).

[6] Yu.F. Zhukovskii, S. Piskunov, J. Begens, J. Kazerovskis, and O. Lisovski. First-principles calculations of point defects in inorganic nanotubes. Phys. Status Solidi B, 2013, 250, p. 793–800.

[7] S. Piskunov, O. Lisovski, J. Begens, D. Bocharov, Yu.F. Zhukovskii, M. Wessel, and E. Spohr. C-, N-, S-, and Fe-doped TiO_2 and $SrTiO_3$ nanotubes for visible-light-driven photocatalytic water splitting: Prediction from first principles. J. Phys. Chem. C, 2015, 119, p. 18686–18696.

[8] A. Chesnokov, O. Lisovski, D. Bocharov, S. Piskunov, Yu.F. Zhukovskii, M. Wessel, and E. Spohr. *Ab initio* simulations on N and S co-doped titania nanotubes for photocatalytic applications. Phys. Scr., 2015, 90, 094013 (p. 1–7).

[9] O. Lisovski, A. Chesnokov, S. Piskunov, D. Bocharov, Yu.F. Zhukovskii, M. Wessel, and E. Spohr. *Ab initio* calculations of doped TiO_2 anatase (101) nanotubes for photocatalytical water splitting applications. Mater. Sci. Semicond. Process., 2016, 42, p. 138–141.

[10] A. Fujishima and K. Honda. Electrochemical photolysis of water at a semiconductor electrode. Nature, 1972, 238, p. 37–38.

[11] Memming, R. Semiconductor Electrochemistry (Wiley-VCH Verlag: Weinheim), 2001.

[12] M. Grätzel. Photoelectrochemical cells. Nature, 2001, 414, p. 338–344.

[13] X. Chen, S. Shen, L. Guo, and S. S. Mao. Semiconductor-based photocatalytic hydrogen generation. Chem. Rev., 2010, 110, p. 6503–6570.

[14] S.G. Kumar and L.G. Devi. Review on modified TiO_2 photocatalysis under UV/visible light: Selected results and related mechanisms on interfacial charge carrier transfer dynamics. J. Phys. Chem. A, 2011, 115, p. 13211–13241.

[15] E. Thimsen, S. Biswas, C.S. Lo, and P. Biswas. Predicting the band structure of mixed transition metal oxides: Theory and experiment. J. Phys. Chem. C, 2009, 113, p. 2014–2021.

[16] T. Bak, J. Nowotny, M. Rekas, and C.C. Sorrell. Photo-electrochemical hydrogen generation from water using solar energy: Materials-related aspects. Int. J. Hydrogen Energy, 2010, 27, p. 991–1022.

[17] E. Borgarello, J. Kiwi, M. Grätzel, E. Pelizzetti, and M. Visca. Visible light induced water cleavage in colloidal solutions of chromium-doped titanium dioxide particles. J. Am. Chem. Soc., 1982, 104, p. 2996–3002.

[18] S. Klosek and D. Raftery. Visible light driven V-doped TiO_2 photocatalyst and its photooxidation of ethanol. J. Phys. Chem. B, 2001, 105, p. 2815–2819.

[19] M. Khan, S. Woo, and O. Yang. Hydrothermally stabilized Fe(III) doped titania active under visible light for water splitting reaction. Int. J. Hydrogen Energy, 2008, 33, p. 5345–5351.

[20] L.G. Devi, N. Kottam, S.G. Kumar, and K.S.A. Raju. Mechanism of charge transfer in the transition metal ion doped TiO_2 with bicrystalline framework of anatase and rutile: Photocatalytic and photoelectrocatalytic activity. Catal. Lett., 2009, 131, p. 612–617.

[21] X. Chen and C. Burda. The electronic origin of the visible-light absorption properties of C-, N- and S-doped TiO_2 nanomaterials. J. Am. Chem. Soc., 2008, 130, p. 5018–5019.

[22] W. Lin, W. Yang, I. Huang, T. Wu, and Z. Chung. Hydrogen production from methanol/water photocatalytic decomposition using Pt/TiO_2-xNx catalyst. Energy Fuel, 2009, 23, p. 2192–2196.

[23] T. Umebayashi, T. Yamaki, H. Itoh, and K. Asai. Band gap narrowing of titanium dioxide by sulfur doping. Appl. Phys. Lett., 2002, 81, p. 454–456.

[24] J.C. Yu, W. Ho, J. Yu, H. Yip, P.K. Wong, and J. Zhao. Efficient visible-light-induced photocatalytic disinfection on sulfur-doped nanocrystalline titania. Environ. Sci. Technol., 2005, 39, p. 1175–1179.

[25] K. Nishijima, T. Kamai, N. Murakami, T. Tsubota, and T. Ohno. Photocatalytic hydrogen or oxygen evolution from water over S- or N-doped TiO_2 under visible light. Int. J. Photoenergy, 2008, 2008, p. 1–7.

[26] S.U.M. Khan, M. Al-Shahry, and W.B. Ingler. Efficient photochemical water splitting by a chemically modified n-TiO_2. Science, 2002, 297, p. 2243–2245.

[27] C. Xu, Y.A. Shaban, W.B. Ingler, and S.U.M. Khan. Nanotube enhanced photoresponse of carbon modified (CM)-*n*-TiO_2 for efficient water splitting. Energy Mater. Sol. Cells, 2007, 91, p. 938–943.

[28] G. Yan, M. Zhang, J. Hou, and J. Yang. Photoelectrochemical and photocatalytic properties of N+S co-doped TiO_2 nanotube array films under visible light irradiation. Mater. Chem. Phys., 2011, 129, p. 553–557.

[29] J. Lv, T. Sheng, L. Su, G. Xu, D. Wang, Z. Zheng, and Y. Wu. N, S co-doped-TiO_2/fly ash beads composite material and visible light photocatalytic activity. Appl. Surf. Sci., 2013, 284, p. 229–234.

[30] G. Wang, Y. Ling, and Y. Li. Oxygen-deficient metal oxide nanostructures for photoelectrochemical water oxidation and other applications. Nanoscale, 2012, 4, p. 6682–6691.

[31] M. Li, J. Zhang, and Y. Zhang. First-principles calculation of compensated (2N, W) co-doping impacts on band gap engineering in anatase TiO_2. Chem. Phys. Lett., 2012, 527, p. 63–66.

[32] R. Asahi, T. Morikawa, T. Ohwaki, K. Aoki, and Y. Taga. Visible-light photocatalysis in nitrogen-doped titanium oxides. Science, 2001, 293, p. 269–271.

[33] D. Zhang and M. Yang. Band structure engineering of TiO_2 nanowires by *n-p* co-doping for enhanced visible-light photoelectrochemical water-splitting. Phys. Chem. Chem. Phys., 2013, 15, p. 18523–18529.

[34] M. Nolan. Electronic coupling in iron oxide-modified TiO_2 leads to a reduced band gap and charge separation for visible light active photocatalysis. Phys. Chem. Chem. Phys., 2011, 13, p. 18194–18199.

[35] A.M. Márquez, J. Plata, Y. Ortega, and J.F. Sanz. Structural defects in W-doped TiO_2 (101) anatase surface: DFT study. J. Phys. Chem. C, 2011, 115, p. 16970–16976.

[36] S.A. Shevlin and S.M. Woodley. Electronic and optical properties of doped and undoped (TiO_2)n nanoparticles. J. Phys. Chem. C, 2010, 114, p. 17333–17343.

[37] Q. Meng, J. Wang, Q. Xie, H. Dong, and X. Li. Water splitting on TiO_2 nanotube arrays. Catal. Today, 2011, 165, p. 145–149.

[38] W.N. Zhao and Z.P. Liu. Mechanism and active site of photocatalytic water splitting on titania in aqueous surroundings. Chem. Sci., 2014, 5, p. 2256–2264.

[39] S.W. Boettcher, J.M. Spurgeon, M.C. Putnam, E.L. Warren, D.B. Turner-Evans, M.D. Kelzenberg, J.R. Maiolo, H.A. Atwater, and N.S. Lewis. Energy-conversion properties of vapor–liquid-solid-grown silicon wire-array photocathodes. Science, 2010, 327, p. 185–187.

[40] N. Beermann, L. Vayssieres, S.-E. Lindquist, and A. Hagfeldt. Photoelectrochemical studies of oriented nanorod thin films of hematite. J. Electrochem. Soc., 2000, 147, p. 2456–2461.

[41] J.M. Macak, M. Zlamal, J. Krysa, and P. Schmuki. Self-organized TiO_2 nanotube layers as highly efficient photocatalysts. Small, 2007, 3, p. 300–304.

[42] M.A. Khan, H. Jung, and O. Yang. Synthesis and characterization of ultrahigh crystalline TiO_2 nanotubes. J. Phys. Chem. B, 2006, 110, p. 6626–6630.

[43] R. Dovesi, V.R. Saunders, C. Roetti, R. Orlando, C.M. Zicovich-Wilson, F. Pascale, B. Civalleri, K. Doll, N.M. Harrison, I.J. Bush, P. D'Arco, M. Llunell, M. Causà, Y. Noël. CRYSTAL14 User's Manual, (University of Torino, 2014). http://www.crystal.unito.it/.

[44] M. Valiev, E.J. Bylaska, N. Govind, K. Kowalski, T.P. Straatsma, H.J.J. Van Dam, D. Wang, J. Nieplocha, E. Apra, T.L. Windus, and W.A. de Jong. NWChem: A comprehensive and scalable open-source solution for large scale molecular simulations. Comput. Phys. Commun., 2010, 181, p. 1477–1489.

[45] R.A. Evarestov. Theoretical Modeling of Inorganic Nanostructures. Symmetry and *Ab initio* Calculations of Nanolayers, Nanotubes and Nanowires, 2015 (Series: Nano-Science and Technology; Springer-Verlag, Berlin-Heidelberg).

[46] A.D. Becke. Density-functional thermochemistry. III. The role of exact exchange. J. Chem. Phys., 1993, 98, p. 5648–5652.

[47] P.J. Hay and W.R. Wadt. *Ab initio* effective core potentials for molecular calculations. Potentials for K to Au including the outermost core orbitals. J. Chem. Phys., 1985, 82, 299–310.

[48] R.A. Evarestov, A.V. Bandura, M.V. Losev, S. Piskunov, and Yu.F. Zhukovskii. Titania nanotubes modeled from 3- and 6-layered (101) anatase sheets: Line group symmetry and comparative *ab initio* LCAO calculations. Phys. E, 2010, 43, p. 266–278.

[49] R.A. Evarestov, Yu.F. Zhukovskii, A.V. Bandura, and S. Piskunov. Symmetry and models of single-wall TiO_2 nanotubes with rectangular morphology. Cent. Eur. J. Phys., 2011, 9, p. 492–501.

[50] R.A. Evarestov, D.B. Migas, and Yu.F. Zhukovskii. Symmetry and stability of the rutile-based TiO_2 nanowires: Models and comparative LCAO plane wave DFT calculations. J. Phys. Chem. C, 2012, 116, p. 13395–13402.

[51] R.A. Evarestov and Yu.F. Zhukovskii. Four-faceted nanowires generated from densely-packed TiO_2 rutile surfaces: *Ab initio* calculations. Surf. Sci., 2013, 608, p. 226–240.

[52] H.J. Monkhorst and J.D. Pack. Special points for Brillouin-zone integrations. Phys. Rev. B, 1976, 13, p. 5188–5192.

[53] U. Diebold. The surface science of titanium dioxide. Surf. Sci. Rep., 2003, 48, p. 53–229.

[54] C.Z. Wen, H.B. Jiang, S.Z. Qiao, H.G. Yang, and G.Q. Lu. Synthesis of high-reactive facets dominated in anatase TiO_2. Chem. Commun., 2011, 21, p. 7052–7061.

[55] M. Lazzeri, A. Vittadini and A. Selloni. Structure and energetics of stoichiometric TiO_2 anatase surfaces. Phys. Rev. B, 2001, 63, 155409 (p. 1–9).

[56] A.M. Ferrari, D. Szieberth, C.M. Zicovich-Wilson, and R. Demichelis. Anatase (001) 3 ML nanotubes, the first TiO_2 nanotube with negative strain energies: A DFT prediction. J. Phys. Chem. Lett., 2010, 1, p. 2854–2857.

[57] J. Sauer. Molecular models in *ab initio* studies of solids and surfaces: From ionic crystals and semiconductors to catalysts. Chem. Rev., 1989, 89, p. 199–255.

[58] D. Berger, A.J. Logsdail, H. Oberhofer, M.R. Farrow, C.R.A. Catlow, P. Sherwood, A.A. Sokol, V. Blum, and K. Reuter. Embedded-cluster calculations in a numeric atomic orbital density-functional theory framework. J. Chem. Phys., 2014, 141, 024105.

[59] A.V. Bandura, R.A. Evarestov, and Yu.F. Zhukovskii. Energetic stability and photocatalytic activity of $SrTiO_3$ nanowires: Ab initio simulations. Royal Soc. Chem. Advances, 2015, 5, p. 24115–24125.

IntechOpen